JACS
JOURNAL OF THE AMERICAN CHEMICAL SOCIETY

ARTICLE

pubs.acs.org/JACS

External-Stimuli Responsive Photophysics and Liquid Crystal Properties of Self-Assembled "Phosphole-Lipids"

Yi Ren, Wang Hay Kan, Matthew A. Henderson, Paolo G. Bomben, Curtis P. Berlinguette, Venkataraman Thangadurai, and Thomas Baumgartner*

Department of Chemistry, University of Calgary, 2500 University Drive NW, Calgary, AB T2N 1N4, Canada

Supporting Information

ABSTRACT: A series of new amphiphilic phosphonium materials that combine the electronic features of phospholes with self-assembly features of lipids were synthesized. Variable concentration/temperature and 2D NMR studies suggested that the systems undergo *intramolecular* conformation changes between a "closed" and "open" form that are triggered by *intermolecular* interactions. The amphiphilic features of the phospholium species also induce liquid crystalline and soft crystal phase behavior in the solid state, which was studied by differential scanning calorimetry (DSC), polarized optical microscopy (POM), and variable temperature powder X-ray diffraction (VT-PXRD). The studies revealed that both conjugated backbones and counteranions work together to organize the systems into different morphologies (liquid crystal/soft crystal). Dithieno[3,2-*b*:2′,3′-*d*]phosphole-based compounds exhibit enhanced emission in the solid state and at low temperature in solution due to aggregation-induced enhanced emission (AIEE). Photoinduced electron transfer (PET) induced via the alkoxybenzyl group at the phosphonium center in the fused-ring systems can be effectively suppressed through intermolecular charge transfer (ICT) processes within the main scaffold of a nonfused system, which was confirmed by static and dynamic fluorescence spectroscopy. The dynamic features of these new materials also endow the systems with external-stimuli responsive photophysical properties that can be triggered by temperature and/or mechanical forces.

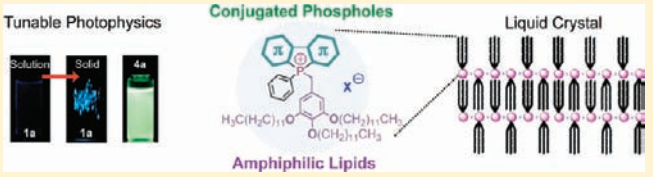

INTRODUCTION

Because of the inherent electronic nature and geometric parameters of the heteroatoms, B-, Si-, P-, and S-containing, π-conjugated systems exhibit intriguing properties that pure carbon-based conjugated derivatives cannot offer to such extent.[1] Consequently, these "heteroatom-doped" systems have increasingly become the focus for the design of highly functional materials in the area of organic/bioelectronics, such as sensors, organic light emitting diodes (OLEDs), organic field-effect transistors (OFETs), and organic photovoltaic cells (OPVs).[2] In the case of phosphorus-based π-conjugated systems, others[2g−k] and we[3] have demonstrated that the phosphorus center can be considered an electronic "switch" for the conjugated moieties (Chart 1) efficiently manipulating the photophysical properties (band gap, fluorescence quantum yield, charge transfer), the redox properties, and electron affinity of the system through a diverse chemistry involving both, modification of E′, such as oxidation (S, O), borylation (BH_3), methylation (Me^+), and metalation (Au, Pd, Pt), as well as the electronic nature of the R groups.[3] More importantly, the phosphorus switch can be tuned reversibly through modification of E′ highlighting the unique features of this class of materials not seen with other heteroatoms.[3a,b]

Because of their tremendous potential, self-assembly properties are a very desirable feature for heteroatom-doped π-conjugated systems with respect to both fundamental studies and practical applications. To install self-assembly features within organic electronic systems, specific intermolecular interactions, such as $\pi-\pi$ interactions, hydrogen bonding, electrostatic interactions, and/or van der Waals forces, can be utilized to organize molecules into well-ordered (1D, 2D, and 3D) micro/nanostructures.[4] Through sophisticated molecular design, ionic interactions that are based on the amphiphilic nature of phospholipid analogues have proven to be a very important and powerful driving force for long-range, high-order, and large-area self-assembly.[5] Ionic liquid crystal systems with well-defined structures and diverse functionalities, in particular, have attracted significant attention recently.[5b,6,7] For example, Kato et al. have reported a series of self-assembled imidazolium salts that self-organize into well-ordered nano/microstructures and show enhanced ionic conductivity, therefore, opening a general path toward practical applications for such systems (Chart 2a).[6]

Mostly due to the synthetic challenges involved, mesomorphic features of inorganic main group element-based (B, Si, P), π-conjugated systems remain fairly limited to date, compared to genuine and nitrogen-based organic species. Weiss and coworkers have carried out pioneering studies on the ionic self-assembly of ammonium and phosphonium compounds that, albeit without involving π-conjugation (Chart 2b), indicated some intriguing features (liquid crystallinity and gelation) that can arise from phosphonium-based systems.[7] Kato's group recently also reported a series of phosphoryl-based systems with

Received: July 20, 2011
Published: September 29, 2011

Chart 1. Heteroatom-Doped π-Conjugated Systems (Left) and Emission of Phosphorus-Based Conjugated Systems Based on the Nature of E′ (Right)

Chart 2. Previously Reported Ionic Compounds and Newly Designed Amphiphilic Phospholes

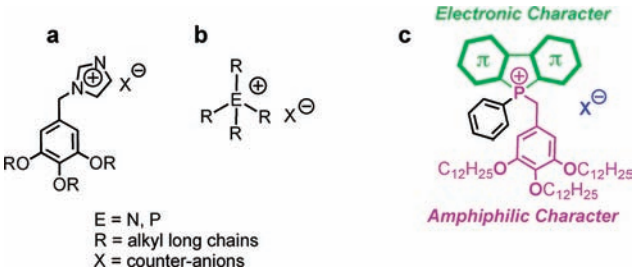

liquid crystalline features.[8] However, to the best of our knowledge, mesomorphic properties and static/dynamic photophysical properties of ionic phosphorus-based conjugated systems have not been systematically studied to date.

In keeping the promising materials mentioned above in mind, we have now targeted a series of novel amphiphilic phospholium materials in this study that combine the electronic character of π-conjugated phospholes with the amphiphilic character of lipids (Chart 2c). The conjugated phosphole backbones were anticipated to provide intriguing photophysical properties, while the amphiphilic lipid-like (hydrophilic head and hydrophobic tail) features could potentially induce micro/nanosegregated bulk structures. Most importantly, we envisioned that highly tunable photophysical properties could also be realized in a unique way exclusively through *dynamic* structural changes, *without* further chemical modification of the new systems. The conformational changes of the molecular species have been comprehensively studied by variable concentration/temperature and 2D NMR experiments, and the liquid crystalline properties of the materials were determined by differential scanning calorimetry (DSC), polarized optical microscopy (POM), and variable temperature powder X-ray diffraction (VT-PXRD); their photophysical properties were characterized by UV−vis and fluorescence spectroscopy (static and time-resolved).

RESULTS AND DISCUSSION

Synthesis and Conformation Studies. The π-conjugated phosphole-containing scaffolds **L1**, **L2**, and **L3**, used for this study, have been synthesized following our reported protocols (Scheme 1).[3a,d,f] **L4** was obtained through the reduction of the corresponding oxide species, which has also been reported by our group.[3b] The variable conjugated backbones ranging from small dithieno- to larger bis(benzo[*b*]thieno)-entities were expected to offer an opportunity for revealing the conjugation effect on both the photophysical and self-assembly properties of the system. It is worth to mention that these phosphonium salts are the first examples of benzyl-substituted phospholium species. The trivalent phospholes were transformed into the corresponding phospholium salts via nucleophilic substitutions with 3,4,5-tris(dodecyloxy)benzyl bromide in refluxing toluene/tetrahydrofuran (THF), and monitored by the observed downfield shift in the ^{31}P NMR spectra. The resulting phospholium bromide species were subsequently purified through column chromatography. The nucleophilic substitutions were also attempted with dodecyl bromide under similar conditions, but did not provide the target phospholium salts, which is probably due to the lower stability of the required primary dodecyl carbocation. Subsequently, the phospholium salts with different counteranions (BF_4^-, BPh_4^-, and OTf^-) were obtained via metathesis with the corresponding metal salts ($AgBF_4$, $NaBPh_4$, and AgOTf). The easy access of counteranions with different geometric and electronic features allowed us to control the mesomorphic properties (vide infra). The identity of all new phospholium salts was confirmed by multinuclear (^{1}H, ^{13}C, and ^{31}P) NMR spectroscopy, high-resolution mass spectrometry, and elemental analysis.

Remarkably, all compounds (**1a**−**d**, **2a**,**b**, **3a**−**c**, and **4a**) show concentration-dependent changes in their ^{1}H NMR spectra in $CDCl_3$ from 10^{-4} to 10^{-2} M (see Supporting Information), which were tentatively assigned to the flexible nature of the benzyl group allowing for conformational changes about the phosphorus center. Figure 1a shows the variable concentration ^{1}H NMR spectra of **2a** in $CDCl_3$ as representative example. Upon increasing the concentration of **2a** from 10^{-4} to 10^{-2} M at 298 K, the proton chemical shifts of H_b and H_e experienced slight upfield shifts, while H_d close the trisalkoxyphenyl ring, experienced a significant downfield shift. In a control experiment using reference compound **2a′** without flexible benzyl group under otherwise similar conditions (10^{-4} to 10^{-2} M at 298 K in $CDCl_3$; Figure S13), the chemical shift of H_d (ca. 8.05 ppm) only experienced a very small change upon increasing the concentration, which strongly suggests that the chemical shift change of H_d in **2a** is due to intramolecular conformational changes. In fact, the ^{31}P NMR signal of **2a** also experiences a downfield shift upon increasing the concentration from 10^{-4} to 10^{-2} M in $CDCl_3$ (Figure 1b), indicating changes of the environment of the phosphorus center.

To better understand the fluxional processes in solution, and to also study the fundamental structural elements of the new systems in the solid state, the model compound **M1** (Scheme 1) without alkoxy-substituents was synthesized. Its solid-state organization revealed important insights into the conformational differences that very likely apply to all of the new phospholium salts, confirming the fluxional nature of the system. Notably, we were able to obtain two different crystal types, blocks and

Scheme 1. Synthesis of Amphiphilic Phospholes

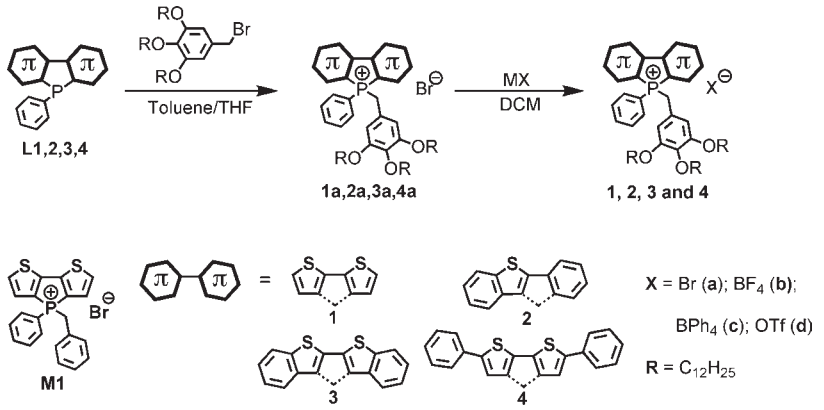

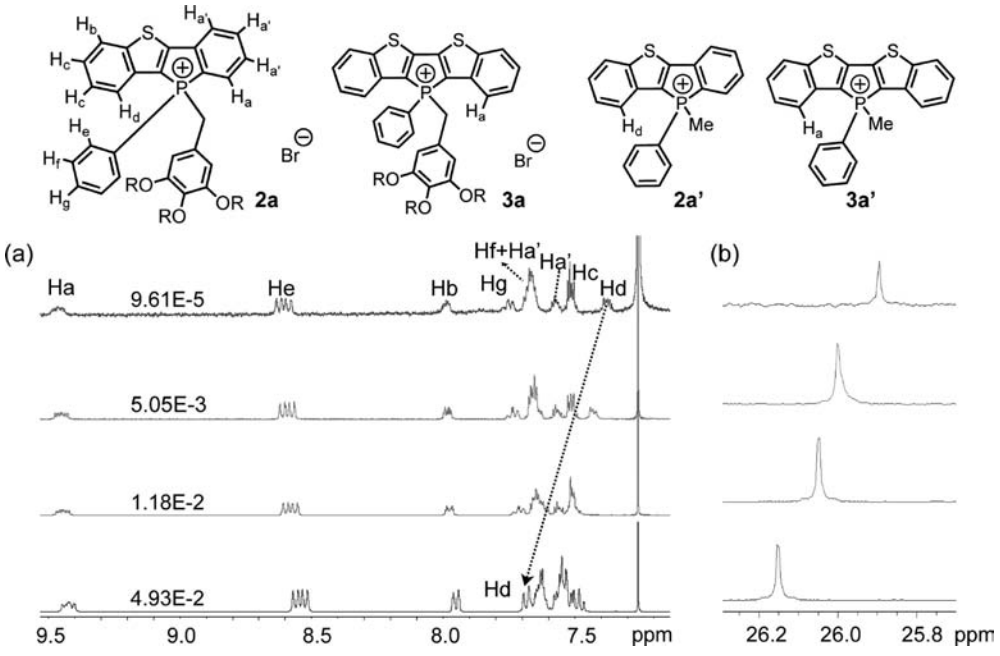

Figure 1. ^{1}H (a) and ^{31}P (b) NMR study of **2a** at varying concentrations ($CDCl_3$, 298 K).

needles, through slow evaporation of different solvents (CH_2Cl_2 or $CHCl_3$) at room temperature, respectively (see Figure 2). In the block-shaped crystals, obtained from CH_2Cl_2, the benzyl ring is close to the main dithieno-scaffold (**M1c**). By contrast, the benzyl ring is removed from the dithieno-scaffold in the needle-shaped crystals obtained from $CHCl_3$ (**M1o**). The existence of both forms of **M1**, closed and open, in the solid state clearly supports the dynamic structural features of these phospholium systems.

For both conformations, hydrogen bonding between the bromide counteranion and the benzylic H-atoms is observed (2.81, 2.94 Å in **M1o** and 2.84, 3.11 Å in **M1c**). In **M1o**, two adjacent dithienophosphole moieties exhibit intermolecular $\pi-\pi$ interactions (3.49 Å); consequently, the distance between the methylene carbon atom (C20) and the central five-membered phosphole plane (C3−C4−C5−C6) is larger in the open conformation of **M1o** (1.618 vs 1.336 Å in **M1c**; see Supporting Information). An ionic interaction between the cationic phospholium center and the anionic bromide was also observed in both structural isomers (**M1c**, $P^+\cdots Br^-$ = 4.34 and 4.45 Å; **M1o**, $P^+\cdots Br^-$ = 4.34 and 4.37 Å), which is comparable to similar phosphonium bromide salts ($P^+\cdots Br^-$: 4.40 Å).[7a] Futhermore, the similar concentration-dependent ^{1}H NMR changes between **M1** and the **1** series further support the hypothesis of the conformation changes in all phospholium species upon increasing the concentration (vide infra).

On the basis of 2D-NMR experiments of compounds **1**−**4** (see Supporting Information) and conformational studies of model compound **M1**, a plausible mechanism for the concentration-dependent conformation changes of this flexible system was proposed (see Figure 3). At low concentration, the alkoxy-substituted benzyl ring is in close proximity to the main scaffold of the π-conjugated moieties (closed form) showing weak intramolecular electrostatic interactions between the electron-poor

dx.doi.org/10.1021/ja206784f |J. Am. Chem. Soc. 2011, 133, 17014–17026

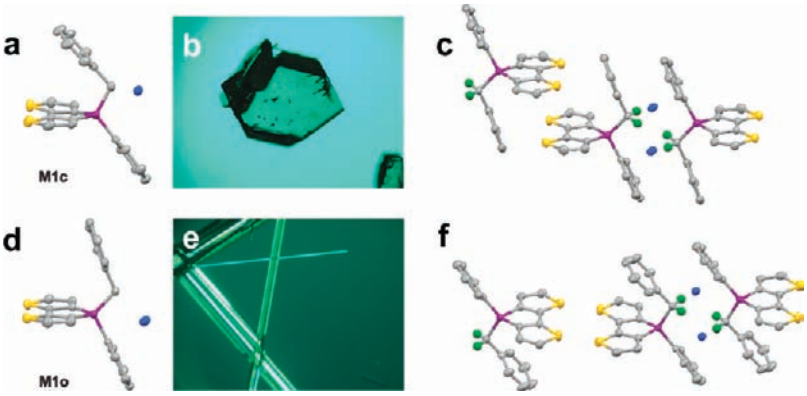

Figure 2. (a) Molecular structure of **M1c** in the solid state (50% probability, H-atoms and solvent molecules omitted for clarity); (b) crystal appearance of **M1c**; (c) molecular packing of **M1c** (benzylic H-atoms are shown in green); (d) molecular structure of **M1o** in the solid state (50% probability, H-atoms omitted for clarity); (e) crystal appearance of **M1o**; (f) molecular packing of **M1o** (benzylic H-atoms are shown in green).

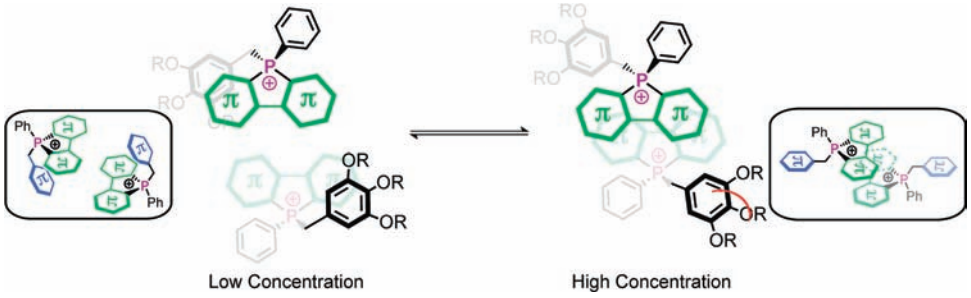

Figure 3. Plausible conformation changes in solution: arrow indicates the trialkoxyl benzyl group leaving away from conjugated phosphole cores (insets: side view of the conformation changes).

conjugated backbone and the electron-rich alkoxy-substituted phenyl ring.[9a,b] At higher concentration, intermolecular interactions (ionic and/or H/$\pi-\pi$) take effect pushing the benzyl group of an adjacent molecule away from the π-conjugated main scaffold (open form), which eliminates the shielding of H_d by the alkoxyphenyl ring.

This process is supported by NOESY NMR experiments carried out at both low (10^{-4} M) and high concentration (10^{-2} M; see Supporting Information). Interestingly, although having a similar environment to H_d in the **2** series, H_a of the symmetric **3** series did not experience a similar shielding from the alkoxyphenyl ring. H_a of **3a** only changed from 8.31 to 8.37 ppm upon increasing the concentration from 10^{-4} to 10^{-2} M at 298 K in $CDCl_3$ (see Supporting Information). These features can be explained by the **3** series adopting a form in which the alkoxy-substituted phenyl ring is not as close as in the **1** series at low concentration, which is probably due to electronic and/or steric effects of the conjugated backbone.[9c,d] Therefore, increasing the concentration did not cause a significant conformation change as observed for the other series.

Similar conformation changes can also be oberserved at different temperatures (see Supporting Information). The NMR studies of the **1** series further confirm that ionic interactions between the π-conjugated cations and the respective counteranions (Br^-, BF_4^-, BPh_4^-, and OTf^-) are influenced by the electronic and geometric nature of the latter (see Supporting Information). Consequently, the systematic studies on the first examples of conjugated benzyl phospholium derivatives clearly support that the discovered dynamic (intra/intermolecular) features can be channeled through the conjugated phosphonium cores as well as the counterions, providing systems with stimuli-responsive and self-assembly properties (vide infra).

Self-Organization in the Solid State. As anticipated, the amphiphilic nature of the phospholium salts indeed offers desirable self-assembly features for the new materials. DSC experiments revealed several thermal phase transitions for each compound (see Figure 4 and Table S1), which were further identified via POM and VT-PXRD experiments.

Generally, oblong and mosaic textures were observed (Figure 5, top; and Supporting Information) for most compounds after cooling from the isotropic state, which are indicative of smectic phases (liquid crystal and soft crystal).[10a] As a general feature for the ionic liquid crystals, dark homeotropic areas were also observed due to the vertical alignments of the compounds between two glass slides.[5b]

As for the **1** series with the smaller conjugated dithienomoiety, smectic liquid crystal properties could be observed for **1a** and **1b** within a very broad temperature range (**1a**, 76−205 °C; **1b**, 41−168 °C; Figure 4), which was further confirmed by VT-PXRD experiments. For example, **1a** with a bromide anion exhibited reflections corresponding to *d*-spacings at 26.1, 13.2, 8.89, and 6.39 Å, which are consistent with the 1:1/2:1/3:1/4 peak ratios characteristic for a lamellar phase (Figure 5).[10b] In addition, a broad peak at the wide angle range (17° ∼ 25°) for **1a** and **1b** (Figure 5 and Supporting Information) indicates the

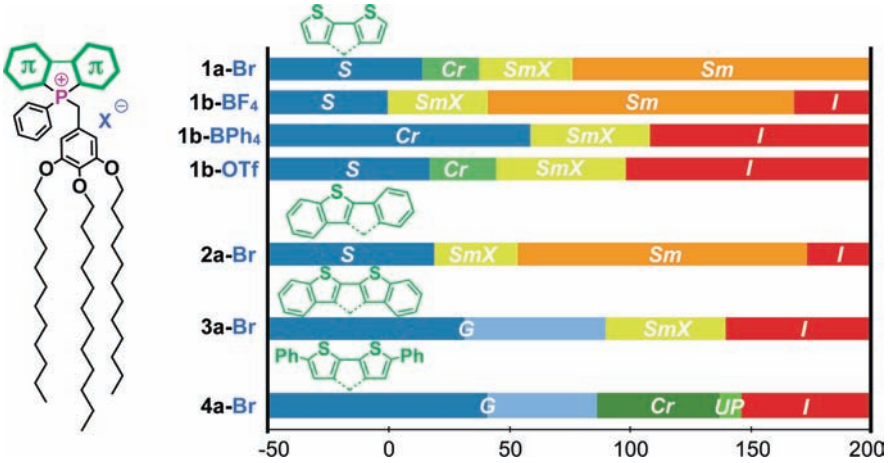

Figure 4. DSC traces of compounds, 2nd heating, 5 °C/min; ***S***, "solid" (precise nature could not be determined due to temperature limitations with the PXRD instrument); ***Cr***, crystalline state; ***SmX***, soft crystal; ***Sm***, smectic phase; ***I***, isotropic liquid; ***UP***, unidentified phase; ***G***, glass transition.

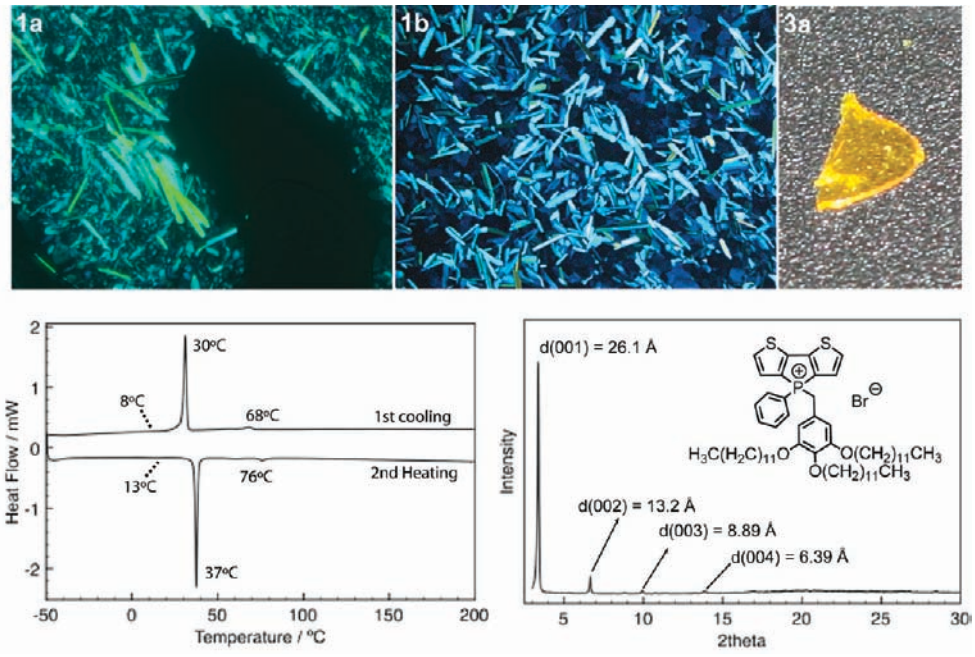

Figure 5. (Top) Polarized optical micrographs of **1a** at 195 °C and **1b** at 168 °C; (top right) glass like solid of **3a** after fast cooling to ca. −20 °C; (bottom left) DSC traces of **1a** with the heating and cooling rate at 5 °C/min (negative heat flow values indicate an endothermic process); (bottom right) powder X-ray diffraction of **1a** at 180 °C.

liquid-like state of the long alkyl chains.[10b] As very important tunable parameter for ionic liquid crystals, the counteranions were also found to impact the molecular organization in the solid state. First, the clearing temperature decreased with the increasing size of counteranions in the order Br^- (205 °C) > BF_4^- (168 °C) > BPh_4^- (108 °C), OTf^- (98 °C). Second, **1c** and **1d** with larger counteranions (OTf^- and BPh_4^-) only exhibited smectic soft crystal phases instead of liquid crystal phases at higher temperature, which was supported by the presence of several weak peaks at wide angle in VT-PXRD experiments (see Supporting Information). These results indicate that the bulkier counteranions exhibit a steric and a more delocalized electronic effect, which suppresses the effective intermolecular ionic interactions.[5b,11] On the basis of the POM and PXRD experiments, the observed liquid crystal phase of these phospholium compounds can very likely be attributed to a Smectic B phase.[10]

In addition to the counteranions, the different conjugated backbones are another important aspect with potential to tune the systems' mesomorphic properties. **2a** with the somewhat extended asymmetric conjugated backbone also exhibits a smectic phase but with a lower clearing point than **1a** (173 vs 205 °C for **1a**). As for **3a**,**b** and **4a**, only soft crystal phases and different crystalline phases can be observed at higher temperatures. Generally, the rigid anisotropic molecular structure can promote efficient molecular alignment in the liquid crystal phase.[10b] The smaller conjugated backbone, such as the dithieno-moiety, can be considered a small spherical shape, which does not diminish the rod-like structural feature of the system combining the

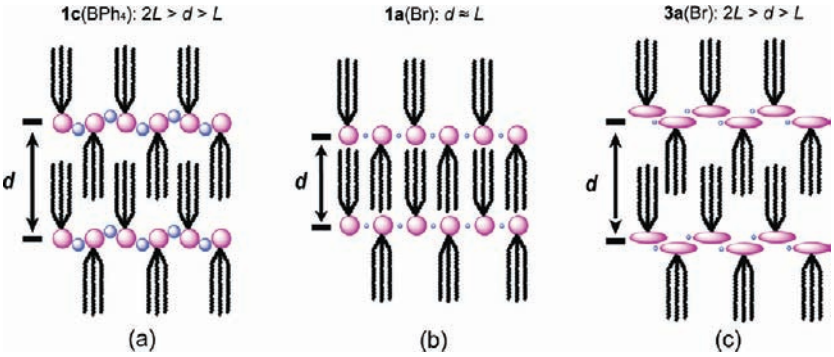

Figure 6. Proposed organization of the phospholium compounds: (a) molecular organization of **1c** in the soft crystal phase; (b) molecular organization of **1a** in the both soft crystal and liquid crystal phase; (c) molecular organization of **3a** in the soft crystal phase (*d*, the thickness of layer; *L*, the length of molecule estimated by theoretical calculation: MM2).

alkoxybenzyl group. As the size of the conjugated backbone increases, the anisotropic features of the molecular structure are diminished; the decreased aspect ratio usually prevents dense molecular packing. This could explain why **2a** exhibits a lower clearing point than **1a**. As the size of conjugated backbone further increases, such as in the case of **3a** and **4a**, the rod-like structural feature is transformed into a T-shape, which destabilizes the mesophase at higher temperatures. Moreover, in **4a** with larger conjugated backbone, the intermolecular ionic interaction could be further weakened through the delocalization of the positive charge within the bulky conjugated backbone.[5b,11] It is worth to mention that **3a**,**b** and **4a** only exhibited very small or broad exothermic transitions during the cooling process and a broad endothermic glass transition in the heating process. These observations indicate that a metastable amorphous state could be induced due to the slow kinetics of crystallization during the cooling process (Figure 5, top right); VT-PXRD indicated that a certain degree of order is still preserved within the amorphous state (see Supporting Information).

According to VT-PXRD experiments (see Supporting Information), most compounds (**1a**−**d**, **2a**, and **3a**) show a lamellar organization in their liquid crystalline state and in the soft crystal phase; the proposed molecular organizations of these compounds are shown in Figure 6. For the **1** series with smaller conjugated moieties, **1a**, **1b** and **1d** show a lamellar structure where the thickness of the layers is close to the length of individual molecule (Table S2) in both liquid crystalline and the soft crystal phase. In addition, the layer thickness decreases with increasing size of the counteranion in the order $Br^- > BF_4^- > OTf^-$, which is probably due to the weakened intermolecular ionic/hydrogen-bonding interactions.[5b,12]

Previous studies of ionic liquid crystal systems have suggested that the intermolecular ionic interaction between cation and anion, as well as halogen-hydrogen bonding within the ionic layer, can stabilize the ordered micro/nanostructures in the mesomorphic phase.[5b,7] NMR spectroscopy and model studies of the new phospholium salts also led us to conclude that the ionic interactions and halogen-hydrogen bonding are the main driving forces for stabilizing the lamellar mesomorphic phase. Therefore, alternating distribution of cation and anion with the alkoxybenzyl rings between adjacent molecules pointing to the opposite direction of ionic layer is proposed for **1a**, **1b**, and **1d** (Figure 6b). Besides, the full interdigitation of alkyl long chains further stabilizes the ionic double layer. In the case of **1c** with the tetraphenylborate anion, an increased layer thickness was observed in the soft crystal phase. This could be explained by stronger intermolecular interactions ($\pi-\pi$ and/or CH-π) between the positive conjugated head and negative tetraphenyl borate that not only reduce the free space within the ionic layer, but also repel the long alkyl chains from adjacent molecules resulting in less interdigitation of the alkyl chains and ultimately lead to the increased layer thickness (Figure 6a). This stronger cation−anion interaction is also supported by the NMR experiments of **1c** (vide supra). **3a** with a more extended conjugated backbone exhibits a layer in the soft crystal phase with a thickness of about 1.4 times of the molecule length. This similar organization is also likely due to intermolecular interactions ($\pi-\pi$ and/or CH$-\pi$) of the conjugated moiety within intralayers (Figure 6c). It is worth to mention that the highly ordered lamellar structures are also preserved at room temperature for some compounds, that is, **1a**−**d** and **2a**. Such well-defined organization in the solid state could potentially enhance the charge-, ion-, and energy-transfer, which are currently investigated in our laboratory.

Photophysical Properties and External Stimuli Responses. *Photophysical Properties.* The varying conjugated backbones further allowed us to systematically study the substituent effect on the photophysical properties of the systems (Table 1). As observed for related phospholes before,[3a,d,f,g] the absorption and emission features are red-shifted by increasing the conjugation length of systems (**1** < **2** < **3** < **4**). Remarkably, the new compounds with the trisalkoxyphenyl ring generally exhibit a blue-shifted emission compared to the methyl derivatives, which is probably due to the higher electron density on the phosphonium center imparted by the donating nature of the benzyl group. Notably, a high fluorescence quantum yield is usually observed for corresponding phosphole oxide (E′ = O) and phospholium (E′ = Me) derivatives (cf.: ϕ_{PL} = 0.3−0.5) in both solution and the solid state, due to the polar/bulky phosphorus center.[3] However, the fused-ring phospholium species (**1**, **2**, and **3** series) were found to only exhibit very low quantum yields (ϕ_{PL} = 0.003−0.005) in CH_2Cl_2. Remarkably, compounds **1a**−**d** exhibit much more intense emission features (ϕ_{PL} = 0.09−0.19) in the solid state (Figure 7) with, for example, ∼40 times enhanced quantum yield for **1c** when compared to its value in solution.

This phenomenon can be related to an aggregation-induced enhanced emission (AIEE), in which intramolecular rotation (IR) of a flexible structural element is restricted in the solid state, leading to increased photoluminescence efficiency.[13] The disappearance of the component with shorter excited-state lifetime (ca. 0.1 ns) in the solid state further supports the restricted

Table 1. Photophysical Properties of the Phospholium Salts

compound	λ_{abs} [nm][a]	ε[L·mol^{-1}·cm^{-1}][b]	λ_{em}[nm] (CH_2Cl_2)	λ_{em}[nm] (solid)	ϕ_{PL} (CH_2Cl_2)[c]	ϕ_{PL} (solid)[c]	τ [ns] (CH_2Cl_2)[d]
M1	372	6384	463	465	0.060	0.60	0.75 (15.59%)
							6.81 (84.41%)
1a	369	12610	454	467	0.0048[e]	0.11	0.11 (66.76%)
							2.72 (8.78%)
							10.78 (24.46%)
1b	369	7250	457	463	0.0031[e]	0.10	0.096 (70.17%)
							9.95 (29.83%)
1c	370	4910	455	458	0.0050[e]	0.19	0.085 (72.01%)
							9.52 (27.99%)
1d	369	9998	456	459	0.0039[e]	0.09	0.099 (72.89%)
							1.70 (4.21%)
							11.51 (22.90%)
2a	337	7710	421[f]	n.d.	n.d.	n.d.	0.025 (7.57%)
							2.26 (5.35%)
							11.21 (87.08%)
2b	339	9040	423[f]	n.d.	n.d.	n.d.	0.019 (19.49%)
							10.12 (80.51%)
3a	415	13470	501	516	0.03	0.05	0.064 (21.80%)
							9.97 (78.20%)
3b	417	14650	503	518	0.04	0.06	0.062 (53.97%)
							8.82 (46.03%)
4a	438	20260	536	538	0.58	0.30	4.90 (35.44%)
							7.56 (64.56%)

[a] The lowest absorption measured in CH_2Cl_2. [b] ε: Molar absorption coefficient. [c] Fluorescence quantum yield was determined by a calibrated integrating sphere system. [d] Fluorescence lifetime. [e] Fluorescence quantum yield cannot be determined by a calibrated integrating sphere system (<0.01), and determined by using quinine sulfate (0.1 M H_2SO_4 solution). [f] Emission spectra measured at ca. 10^{-4} M CH_2Cl_2 due to the low intensity, others measured at ca. 10^{-5} M in CH_2Cl_2. n.d. : not detectable.

intramolecular rotations for **1a**−**d** (see Table S3 in the Supporting Information).[13] In addition, model compound **M** (ϕ_{PL} = 0.06 in CH_2Cl_2; ϕ_{PL} = 0.60 in the solid) with the simple benzyl group, exhibits a stronger emission in both solution and the solid state than the **1** series compounds with the trisalkoxybenzyl group (ϕ_{PL} = 0.003−0.005 in CH_2Cl_2; ϕ_{PL} = 0.10−0.20 in the solid). Such observation suggests that the photoinduced electron transfer (PET) from the alkoxybenzene (donor) to the phospholium

chromophore's main scaffold (acceptor) is likely another nonradiative decay channel.[14] However, it seems that such PET channel is suppressed for the **1** series in the solid state due to the conformational changes, as indicated by the NMR studies (vide supra). Quite different from the **1** series, the quantum yields for the compounds of the **2** series are too low to be detected in either CH_2Cl_2 or the solid state. This observation suggests that intra or/intermolecular PET is still active in the **2** series in the solid state, despite the IR process being naturally restricted. Compounds **3a** and **3b** exhibit relatively higher quantum yields in solution (**3a**, ϕ_{PL} = 0.03; **3b**, ϕ_{PL} = 0.04) than their congeners of the **1** and **2** series, probably due to the different electronic (redox potential, band gap of their conjugated acceptor backbone) or geometric parameters (distance between the donor and acceptor moiety; structural flexibility), likely suppressing PET and/or IR processes.[14] On the other hand, both **3a** and **3b** show enhanced emission in the solid state. By contrast, compound **4a** with the nonfused, extended π-conjugated moiety shows a significantly higher quantum yield in CH_2Cl_2 (ϕ_{PL} = 0.58) and the solid state (ϕ_{PL} = 0.30) compared to the other species in this study. Importantly, however, the structural flexibility of the benzyl unit is still preserved in **4a** according to the NMR studies. Moreover, the higher quantum yield in solution and absence of the shorter excited-state lifetime (τ_1 = 4.90 ns, τ_2 = 7.56 ns) component suggests that the PET is not active in **4a**.

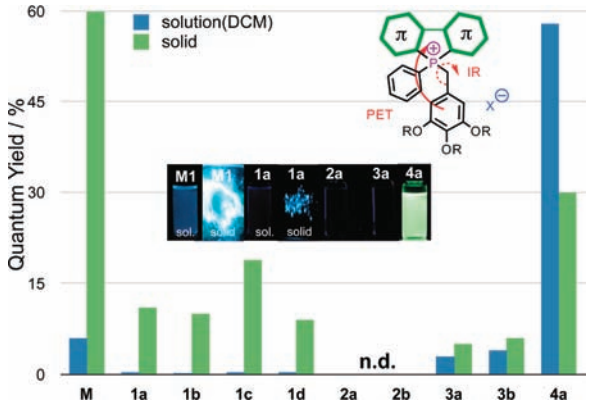

Figure 7. Quantum yields of the phospholium species **M1** and **1**−**4**; (inset top right) plausible nonradiative decay channels (IR = Intramolecular Rotation; PET = Photoinduced Electron Transfer); (inset center) fluorescence pictures of selected compounds in CH_2Cl_2 and the solid state; n.d., not detectable.

To gain some deeper understanding for the observed photophysics, we have performed time-dependent (TD) DFT-calculations at the B3LYP/6-31G(d) level of theory using a PCM-solvation model to counterbalance the omission of the anions in the calculations.[15] To furthermore reduce the computation time, the dodecyloxy moieties were truncated with methoxy groups (Figure 8). We found that all model compounds (**1**$^{\#}$, **2**$^{\#}$, **3**$^{\#}$ and **4**$^{\#}$) show the typical $\sigma^*-\pi^*$ orbital coupling of dithienophospholes in the LUMO orbital.[3] For the fused-ring compounds **1**$^{\#}$ and **3**$^{\#}$, HOMO-1 and HOMO energy levels are very close (ca. 0.1 eV), and fully degenerate for **2**$^{\#}$ according to the TD-DFT calculations. It is worth to mention that, both HOMO and HOMO-1 of **2**$^{\#}$ are mainly localized in electron-rich trimethoxybenzyl ring, while only the HOMO of **1**$^{\#}$ shows a similar distribution; by contrast the HOMO-1 represents the π-conjugated scaffold. However, both HOMO and HOMO-1 of **3**$^{\#}$ show a strong contribution from the conjugated backbone as well as the benzyl group, which is believed to be one major reason for the different observed quantum yields (**3** series > **1** series > **2** series) in solution. Importantly, the HOMO representing the conjugated backbone is significantly destabilized in compound **4**$^{\#}$ due to the extension of the π-system by the terminal phenyl rings, as commonly observed for such materials.

Furthermore, based on the TD-DFT calculations, a weak charge-transfer character within the conjugated backbone of **4**$^{\#}$ can also be found from the outer phenyl rings as weak donors (HOMO) to the centeral phospholium as an acceptor (LUMO). The stabilized HOMO-1, representing the electron-rich trimethoxybenzyl ring in **4**$^{\#}$, suggests that PET is indeed suppressed

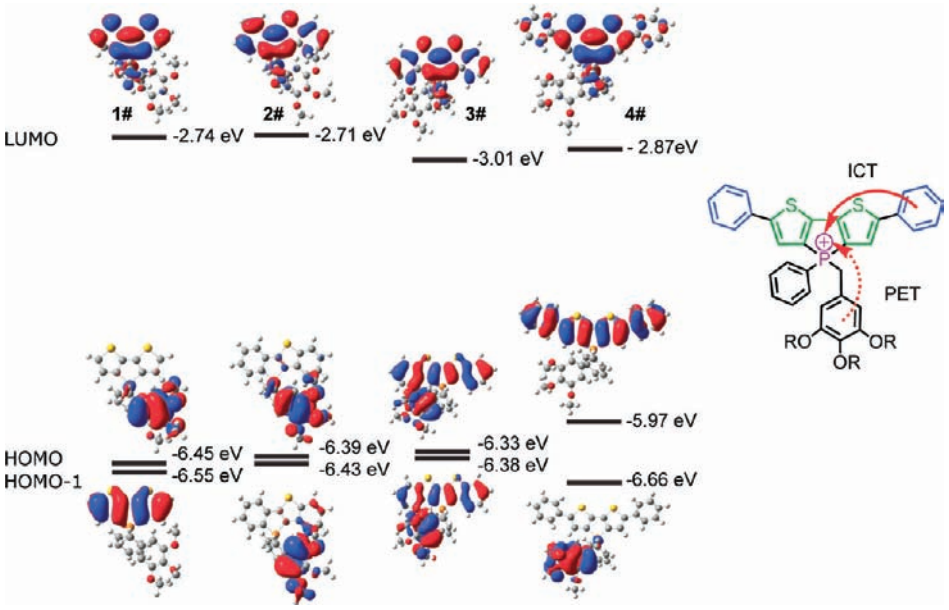

Figure 8. Frontier orbitals of model compounds **1**$^{\#}$, **2**$^{\#}$, **3**$^{\#}$, and **4**$^{\#}$ (B3LYP/6-31G(d), PCM (solvent = dichloromethane)).[15] PET = Photoinduced Electron Transfer; ICT = Intramolecular Charge Transfer.

in this system. The theoretical results further support that this weak intramolecular charge transfer competes with the excited state electron transfer in **4a**, leading to the higher luminescence quantum yield for **4a** when compared to the other phospholium species (Figure 8; Table S4, Supporting Information).

In the solid state, both counteranions and conjugated moieties were found to have a significant impact on the overall emission properties of the materials (Figure 9). The increasing size of the counteranions ($Br^- < BF_4^- < BPh_4^-$, OTf^-) clearly reduces the shifts between the emission wavelengths in solution and the solid state (**1a**, $\Delta\lambda_{em}$ = 13 nm; **1b**, $\Delta\lambda_{em}$ = 6 nm; **1c**, $\Delta\lambda_{em}$ = 3 nm; **1d**, $\Delta\lambda_{em}$ = 3 nm), due to reduced intermolecular interactions of the π-conjugated moieties. The higher quantum yield of **1c** in the solid state also supports the less efficient intermolecular electronic communication due to the much bulkier counteranion (BPh_4^-). On the other hand, both **3a** and **3b** show a more pronounced red shift in the solid-state emission (**3a**, $\Delta\lambda_{em}$ = 15 nm; **3b**, $\Delta\lambda_{em}$ = 15 nm), which could be correlated with more efficient intermolecular $\pi-\pi$ interactions of the larger, more exposed π-conjugated main scaffold. To our surprise, however, the solid-state emission wavelength of **4a** (λ_{em} = 538 nm) with extended phenyl groups is almost the same as in solution (λ_{em} = 536 nm). Compared to **3a**,**b** with a comparable effective conjugation length, the different emission features of **4a** could be explained by less efficient planarization of the conjugated backbone and intermolecular association in the solid state, which are due to twisted terminal phenyl rings[3b] and the bulky pyramidal phospholium center.

External Stimulus Response. The flexible nature of the systems was also reflected in the observed temperature-dependent emission properties (see Supporting Information). All compounds exhibit a hyperchromic emission at 213 K (for **1a**−**d** about 30 times) compared to the intensity at 298 K, likely due to restricted intramolecular rotation at low temperature (Figure 10).[13] It needs to be mentioned that the overall less enhanced emission of **4a** (compared to the other congeners) indicates that intramolecular rotation is not a effective quenching channel, as opposed to the **1** series compounds, probably due to the steric interaction between the bulky trisalkoxybenzyl ring and the twisted terminal phenyl rings in **4a**. Upon reducing the temperature from 298 to 213 K, compounds **2a** and **3a** furthermore show a ∼20 nm, or ∼10 nm red shift in CH_2Cl_2, respectively (Figure 11). Remarkably, the thermal emission responses of the **1** (ca. 7 nm), the **2** (ca. 19 nm), and the **3** series (ca. 10 nm) exhibit a comparable red shift to the chemical modification of the phosphorus center in the **P1** (14 nm), **P2** (17 nm), and **P3** (22 nm) systems reported before (Figure 11).[3a,d,f]

The red-shifted emission at such low concentration (10^{-5} M) is very likely due to the intramolecular conformation changes rather than intermolecular associations, which are further supported by VT NMR experiments of the **1**, **2**, and **3** series (see Supporting Information). Recalling the typical coupling in silole and phosphole species between the σ^*-orbital of exocyclic heteroatom (Si/P)-carbon bonds and the π^*-orbital of the conjugated backbones, this red-shifted emission can be attributed to the change of the $\sigma^*-\pi^*$ orbital overlap during the conformational changes.[3,16]

Flexible structures are known to induce polymorphism in the solid state. Moreover, the transition between the stable and the metastable state triggered through external (thermal and mechanical) stimuli can also induce altered photophysical properties that have drawn a lot attention recently.[17] Remarkably, compound **4a** was also found to show an intriguing mechanical photoluminescence response in the solid state. Upon grinding the solid powder of **4a** deposited on a glass slide, its fluorescence changed from green (λ_{em} = 538 nm, τ = 3.89) to yellow (λ_{em} = 560 nm, τ = 2.70 (7.51%), τ_2 = 7.67 (92.49%); Figure 12, left). Importantly, the original green fluorescence features could be recovered after thermal annealing (ca. 80 °C) and this process (ca. $\Delta\lambda_{em}$ = 20 nm) could be repeated several times without compromising the response (Figure 12, right). To emphasize the unique behavior of **4a**, the fused systems **1a**,**b**, **2a**,**b**, and **3a**,**b** with smaller conjugated cores and counteranions did not exhibit any significant mechanically responsive emission under similar conditions, which supports a possible eximer formation for **4a** upon mechanical grinding potentially accessible via a planarized extended conjugated backbone.

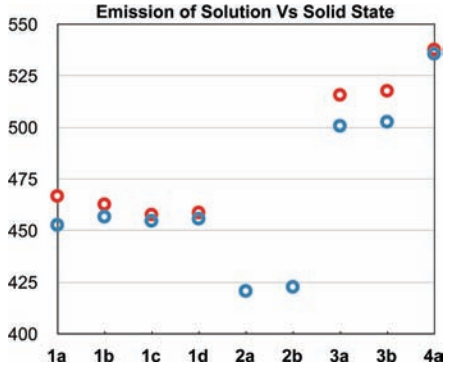

Figure 9. Solution vs solid-state emission (red circle, solid state; blue circle, CH_2Cl_2 solution).

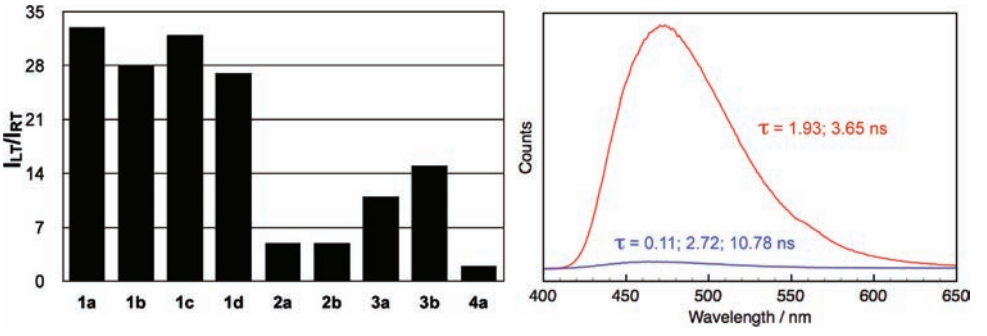

Figure 10. (Left) Emission intensity ratio between 213 and 298 K; (right) emission spectrum of **1a** in 10^{-5} M CH_2Cl_2 solution (red, at 213 K; blue, at 298 K).

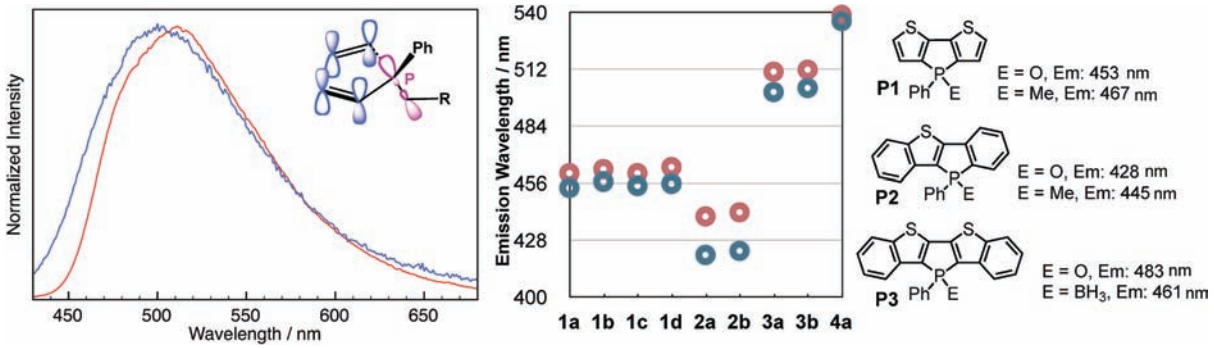

Figure 11. (Left) Normalized emission of **3a** in CH_2Cl_2 10^{-5} M solution (red, at 298 K; blue, at 213 K); (middle) emission wavelengths in 10^{-5} M CH_2Cl_2 solution (red, at 213 K; blue, at 298 K); (right) emission changes through the chemical modification on the phosphorus in **P1**, **P2**, and **P3** systems.

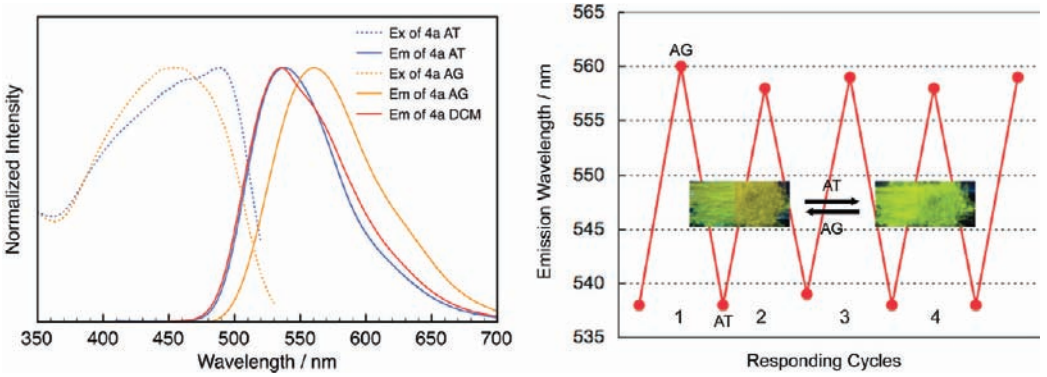

Figure 12. (Left) Excitation (ex, dots) and emission (em, solid) spectra of **1b**; (right) responding cycles; AT = after thermal annealing; AG = after grinding.

To elucidate the mechanism for the mechanochromism of **4a**, variable concentration ^{1}H NMR spectroscopy in $CDCl_3$ was performed that confirmed a similar behavior as observed for the other compounds indicating the alkoxybenzyl ring moving away from π-conjugated main scaffold upon intermolecular association-induced conformation change (Figure 13a). 2D-NOESY experiments (see Supporting Information) also revealed an interaction between H_a and H_i at lower concentration (8.71×10^{-4} M), and a different H_e—H_i interaction at higher concentration (1.12×10^{-2} M). Consistent with the concentration-dependent NMR experiments, both absorption and emission spectra of **4a** showed a noticeable red-shifted shoulder peak upon increasing the concentration (Figure 13b,c). Such red-shifted shoulder was not observed in **1a**, **2a**, and **3a** indicating that the intermolecular interactions may play a role in this concentration-dependent emission.

Further insights on a plausible mechanism for this mechanical response were obtained from the solid-state photophysical properties of two isomers of the model compound **M1** (Figure 14, left). The crystals of **M1c** (cocrystallized with CH_2Cl_2) show intense blue emission (λ_{em} = 456 nm, τ = 7.94 ns). A notable red shift ($\Delta\lambda_{em}$ = 9 nm) was observed for its structural isomer **M1o** (cocrystallized with $CHCl_3$; λ_{em} = 465 nm, τ = 9.90 ns) that can be attributed to the intermolecular interactions in **M1o** (vide supra). TD-DFT calculations performed on the dimers of each isomer (**M1o** and **M1c**), using the X-ray crystallographic data as input, also confirmed the intermolecular orbital coupling in the dimer of **M1o** (Figure 14, middle). It is worth to mention that the emission of **M1** in CH_2Cl_2 (λ_{em} = 461 nm, τ_1 = 0.75 ns, τ_2 = 6.81 ns) is also red-shifted and broadened compared to the emission of isomer **M1o** in the crystal state, which can be considered as sum of the two isomers' emissions in the crystals (Figure 14, left). Notably, mechanical force also caused the emission changes for the two **M1** isomer crystals (see Supporting Information). These results indicate that (i) strong intermolecular π—π interactions could induce an excimer emission even with the bulky phosphonium center, (ii) emission in solution reflects the average emission of the different isomers that is consistent with the multiexponential decay of **1**, **2**, **3**, and **4** series, and (iii) different conformations of the flexible phospholium species can lead to a different emission wavelengths, which can be triggered through mechanical forces.

To reveal the nature of the intermolecular interactions in the solid state, PXRD experiments of **4a** were carried out before and after mechanical grinding. As shown in Figure 14 (right), the mechanical force induces a completely different PXRD pattern. Moreover, the significantly reduced diffraction intensity indicates that **4a** becomes more amorphous upon mechanical grinding. Similar observations could also be detected in other mechanically responsive systems.[17] Finally, **4a** was also doped into a polystyrene (PS) matrix at different concentrations (0.05—20 wt %) to solidify intra/intermolecular interactions in the solid state as cause for the red-shifted photophysics. For the higher doping concentration (20 wt.%), the polymer matrix shows similar absorption and emission to **4a** in solution (see Supporting Information). However, the 0.05% doped polymer matrix shows a noticeably blue-shifted emission (λ_{em} = 529 nm, τ_1 = 3.37 ns, τ_2 = 6.62 ns) compared to the

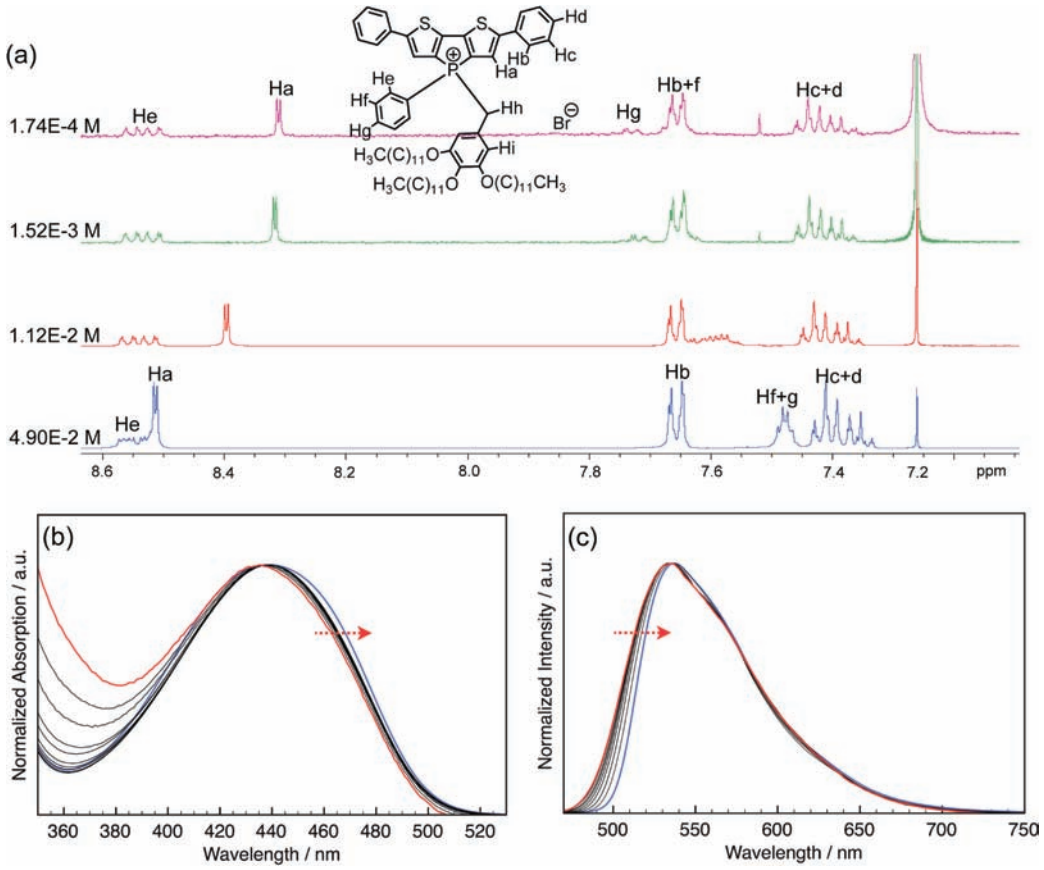

Figure 13. (a) Concentration-dependent ^{1}H NMR spectra of **4a** ($CDCl_3$); (b) concentration-dependent absorption spectra of **4a**, 10^{-3} M (blue line) $\sim 10^{-9}$ M (red line) in $CHCl_3$; (c) concentration-dependent emission spectra of **4a** 10^{-3} M (blue line) $\sim 10^{-9}$ M (red line) in $CHCl_3$.

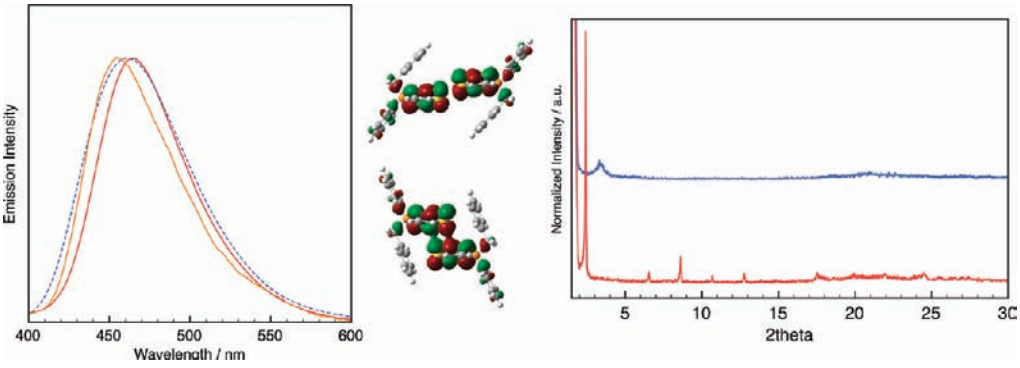

Figure 14. (Left) Emission spectra of model **M1** (blue dash, emission in 10^{-6} M CH_2Cl_2 solution; orange, emission **M1o** (crystal); red, emission **M1c** (crystal). (Middle) Differences in intermolecular orbital coupling of **M1o** (top) and **M1c** (bottom). (Right) PXRD of **4a**; red, before grinding; blue, after grinding.

20% doped matrix (λ_{abs} = 536 nm, τ_1 = 2.23 ns, τ_2 = 4.38 ns; see Supporting Information). At the low concentration level (0.05 wt %), the blue-shifted emission of **4a** can be rationalized as monomer emission with trapped conformation in the polymer matrix as opposed to the higher degree freedom of the monomer in solution, which is consistent with model studies.

On the basis of these studies, the mechanism of the mechanically responsive emission of **4a** as shown in Figure 15 is proposed. Upon mechanical grinding, adjacent molecules come close to each other (with adjacent conjugated cores coming together and the trisalkoxybenzyl group moving away) through cooperative intermolecular interactions (ionic and/or H/$\pi-\pi$), which potentially induces excimer emission; in turn, the terminal phenyl rings are consequently forced into a more planar conformation with restricted motion, resulting in the red-shifted emission. During thermal annealing, the motion of the flexible trisalkoxybenzyl ring likely provides more free space for twisting of the terminal phenyl rings resulting in an interruption of the conjugation. This motion can also interrupt the excimer formation in the solid state via pushing adjacent conjugated phosphonium cores away from each

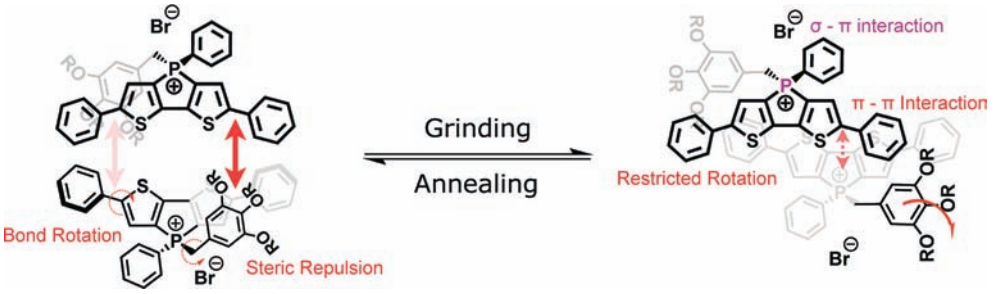

Figure 15. Proposed mechanism for the mechanical and thermal response of **4a**.

other.[3g] According to NMR spectroscopy and the polymer matrix studies, however, a change in the $\sigma-\pi$ interaction can also not be fully ruled out at the current stage.

CONCLUSIONS AND REMARKS

In conclusion, we have synthesized a series of novel "phosphole-lipids" combining both conjugated phosphole backbones and amphiphilic lipid structures through very effective phosphorus chemistry approaches. The amphiphilic character of the new species allowed accessing self-assembly features, as well as intriguing photophysical properties. Systematic NMR studies (^{1}H, ^{31}P, VT, VC, 2D) suggested that these newly synthesized flexible systems undergo conformational changes from "closed" to "open" forms via increasing concentration or temperature, respectively. The isomeric structures of the model compound **M1** further support the proposed conformational changes. Our results reveal that the intermolecular ionic interaction is a very effective driving force for stabilizing lamellar liquid crystal and soft crystal phases in these ionic phosphorus-based π-conjugated systems. The well-preserved and highly ordered organization of these systems at room temperature make them very promising candidates for the application of organic electronics. The newly discovered dynamic structural features induce an unusual enhanced emission for the **1** series compounds in the solid state (up to 40 times for **1c**) due to aggregation-induced enhanced emission (AIEE). We have shown that, through careful molecular design, the fluorescence of the system (such as **4a**) can be significantly enhanced via an intramolecular charge transfer within the conjugated backbone in both solution (ϕ_{PL} = 58%) and the solid state (ϕ_{PL} = 30%). DFT calculations also supported the photophysical processes occurring in these systems. Importantly, these flexible structures endow the system with very interesting thermally responsive emission in solution that is comparable to the chemical modification of phosphorus center. In the solid state, **4a**, with extended conjugated backbone, also displays a mechanically responsive emission that can be switched back via thermal treatment.

These initial studies have successfully demonstrated that "smart phospholes" can be realized through sophisticated molecular engineering of the dynamic features on the *phosphorus center*, providing unique photophysical and self-assembly properties for phosphorus-based conjugated materials that can be modified through external stimuli (temperature/concentration, or host and guest interaction). However, in order to further amplify the external stimuli response (absorption and emission), the $\sigma-\pi$ orbital coupling likely needs to be maximized, and further engineering toward efficient intermolecular interactions are also required, which is currently under detailed investigation in our laboratory, as these well-organized structures could potentially enhance energy-, charge-, and ion-transfer processes that are highly desirable for practical applications.

ASSOCIATED CONTENT

Supporting Information. Full experimental details for the synthesis of all new compounds. Additional ^{1}H, ^{31}P, VC/VT and 2D NMR data, TD-DFT data, photophysical data, DSC traces, POM images, VT-PXRD data; complete ref 15. CIF files of all structures determined by X-ray crystallography and intermolecular packing interactions of all crystallographically characterized compounds. This material is available free of charge via the Internet at http://pubs.acs.org.

AUTHOR INFORMATION

Corresponding Author
Thomas.baumgartner@ucalgary.ca

ACKNOWLEDGMENT

Financial support by NSERC of Canada and the Canada Foundation for Innovation (CFI) is gratefully acknowledged. We also thank Alberta Ingenuity now part of Alberta Innovates - Technology Futures for a graduate scholarship (Y.R.) and a New Faculty Award (T.B.). Thanks to Prof. T. Sutherland for helpful discussions with regard to the liquid crystal properties.

REFERENCES

(1) *Boron:*(a) Mercier, L. G.; Piers, W. E.; Parvez, M. *Angew. Chem., Int. Ed.* **2009**, *48*, 6108–6111. (b) Caruso, A., Jr.; Tovar, J. D. *Org. Lett.* **2011**, *13*, 3106–3109. (c) Wakamiya, A.; Mori, K.; Yamaguchi, S. *Angew. Chem., Int. Ed.* **2007**, *46*, 4273–4276. (d) Yamaguchi, S.; Akiyama, S.; Tamao, K. *J. Am. Chem. Soc.* **2001**, *123*, 11372–11375. (e) Elbing, M.; Bazan, G. C. *Angew. Chem., Int. Ed.* **2008**, *47*, 834–838. *Silicon:* (f) Yamaguchi, S.; Tamao, K. *J. Chem. Soc., Dalton Trans.* **1998**, 3693–3702. (g) Zhan, X.; Barlow, S.; Marder, S. R. *Chem. Commun* **2009**, 1948–1955. (h) Zhan, X.; Risko, C.; Amy, F.; Chan, C.; Zhao, W.; Barlow, S.; Kahn, A.; Brédas, J.-L.; Marder, S. R. *J. Am. Chem. Soc.* **2005**, *127*, 9021–9029. (i) Yamaguchi, S.; Xu, C.; Tamao, K. *J. Am. Chem. Soc.* **2003**, *125*, 13662–13663. (j) Xu, C.; Wakamiya, A.; Yamaguchi, S. *J. Am. Chem. Soc.* **2005**, *127*, 1638–1639. *Phosphorus:*(k) Fukazawa, A.; Yamaguchi, S. *Chem.—Asian J.* **2009**, *15*, 1386–1400. (l) Baumgartner, T; Réau, R. *Chem. Rev.* **2006**, *106*, 4681–4727. correction: *Chem. Rev.* **2007**, *108*, 303. (m) Dillon, K. B.; Mathey, F.; Nixon, J. F. *Phosphorus: The Carbon Copy*; Wiley: New York, 1998. (n) Mathey, F. *Phosphorus-Carbon Heterocyclic Chemistry: The Rise of a New Domain*; Pergamon Press: Amsterdam, 2001. *Sulfur:*(o) Curtis, M. D.; Cao, J.; Kampf, J. W. *J. Am. Chem. Soc.* **2004**, *126*, 4318–1055. (p) Kim, E.-G.; Coropceanu, V.; Gruhn, N. E.; Sánchez-Carrera, R. S.; Snoeberger, R.;

Matzger, A. J.; Brédas, J.-L. *J. Am. Chem. Soc.* **2007**, *129*, 13072–13081. (q) Suzuki, Y.; Okamoto, T.; Wakamiya, A.; Yamaguchi, S. *Org. Lett.* **2008**, *10*, 3393–3396. (r) Amir, E.; Rozen, S. *Angew. Chem., Int. Ed.* **2005**, *44*, 7374–7378. (s) Barbarella, G.; Favaretto, L.; Zambianchi, M.; Pudova, O.; Arbizzani, C.; Bongini, A.; Mastragostino, M. *Adv. Mater.* **1998**, *10*, 551–554. (t) Tedesco, E.; Sala, F. D.; Favaretto, L.; Barbarella, G.; Albesa-Jové, D.; Pisignano, D.; Gigli, G.; Cingolani, R.; Harris, K. D. M. *J. Am. Chem. Soc.* **2003**, *125*, 12277–122783.

(2) *Boron:*(a) Jäkle, F. *Chem. Rev.* **2010**, *110*, 3985–4022. (b) Wade, C. R.; Broomsgrove, A. E. J.; Aldridge, S.; Gabbaï, F. P. *Chem. Rev.* **2010**, *110*, 3958–3984. (c) Hudson, Z. M.; Wang, S. *Acc. Chem. Res.* **2009**, *42*, 1548–1596. *Silicon:*(d) Chu, T.-Y.; Lu, J.; Beaupré, S.; Zhang, Y.; Pouliot, J.-R.; Wakim, S.; Zhou, J.; Leclerc, M.; Li, Z.; Ding, J.; Tao, Y. *J. Am. Chem. Soc.* **2011**, *125*, 4250–4253. (e) Hou, J.; Chen, H.-Y.; Zhang, S.; Li, G.; Yang, Y. *J. Am. Chem. Soc.* **2008**, *130*, 16144–16145. (f) Sohn, H.; Sailor, J. M.; Magde, D.; Trogler, W. C. *J. Am. Chem. Soc.* **2003**, *125*, 3821–3830. *Phosphorus:*(g) Matano, Y.; Saito, A.; Fukushima, T.; Tokudome, Y.; Suzuki, F.; Sakamaki, D.; Kaji, H.; Ito, A.; Tanaka, K.; Imahori, H. *Angew. Chem., Int. Ed.* **2011**, *50*, 8016–8020. (h) Romero-Nieto, C.; Durben, S.; Kormos, I. M.; Baumgartner, T. *Adv. Funct. Mater.* **2009**, *19*, 3625–3631. (i) Fadhel, O.; Gras, M.; Lemaitre, N.; Deborde, V.; Hissler, M.; Geffroy, B.; Réau, R. *Adv. Mater.* **2009**, *21*, 1261–1265. (j) Tsuji, H.; Sato, K.; Sato, Y.; Nakamura, E. *J. Mater. Chem.* **2009**, *19*, 3364–3366. (k) Su, H.-C.; Fadhel, O.; Yang, C.-J.; Cho, T.-Y.; Fave, C.; Hissler, M.; Wu, C.-C.; Réau, R. *J. Am. Chem. Soc.* **2006**, *128*, 983–995. (l) Fave, C.; Cho, T.-Y.; Hissler, M.; Chen, C.-W.; Luh, T.-Y.; Wu, C.-C.; Réau, R. *J. Am. Chem. Soc.* **2003**, *125*, 9254–9255. *Sulfur:*(m) Xiao, K.; Liu, Y.; Qi, T.; Zhang, W.; Wang, F.; Gao, J.; Qiu, W.; Ma, Y.; Cui, G.; Chen, S.; Zhan, X.; Yu, G.; Qin, J.; Hu, W.; Zhu, D. *J. Am. Chem. Soc.* **2005**, *127*, 13281–13286.

(3) (a) Ren, Y.; Baumgartner, T. *J. Am. Chem. Soc.* **2011**, *133*, 1328–1340. (b) Dienes, Y.; Durben, S.; Kárpáti, T.; Neumann, T.; Englert, U.; Nyulászi, L.; Baumgartner, T. *Chem.—Eur. J.* **2007**, *13*, 7487–7500. (c) Ren, Y.; Baumgartner, T. *Chem.—Asian J.* **2010**, *5*, 1918–1929. (d) Baumgartner, T.; Neumann, T.; Wirges, B. *Angew. Chem., Int. Ed.* **2004**, *43*, 6197–6201. (e) Durben, S.; Dienes, Y.; Baumgartner, T. *Org. Lett.* **2006**, *8*, 5893–5893. (f) Dienes, Y.; Eggenstein, M.; Kárpáti, T.; Sutherland, T. C.; Nyulászi, L.; Baumgartner, T. *Chem.—Eur. J.* **2008**, *14*, 9878–9889. (g) Ren, Y.; Dienes, Y.; Hettel, S.; Parvez, M.; Hoge, B.; Baumgartner, T. *Organometallics* **2009**, *28*, 734–740. (h) Romero-Nieto, C.; Kamada, K.; Cramb, D. T.; Merino, S.; Rodríguez-López, J.; Baumgartner, T. *Eur. J. Org. Chem.* **2010**, *27*, 5225–5231. (i) Durben, S.; Linder, T.; Baumgartner, T. *New J. Chem.* **2010**, *34*, 1585–1592. (j) Romero-Nieto, C.; Merino, S.; Rodríguez-López, J.; Baumgartner, T. *Chem.—Eur. J.* **2009**, *15*, 4135–4145.

(4) (a) Zhang, L.; Che, Y.; Moore, J. S. *Acc. Chem. Res.* **2008**, *41*, 1596–1608. (b) Hoeben, F. J. M.; Jonkheijm, P.; Meijer, E. W.; Schenning, A. P. H. J. *Chem. Rev.* **2005**, *105*, 1491–1546. (c) Diegelmann, S. R.; Gorham, J. M.; Tovar, J. D. *J. Am. Chem. Soc.* **2008**, *130*, 13840–13841. (d) Guerzo, A. D.; Olive, A. G. L.; Reichwagen, J.; Hopf, H.; Desvergne, J.-P. *J. Am. Chem. Soc.* **2005**, *127*, 17984–17985. (e) Ajayaghosh, A.; Praveen, V. K. *Acc. Chem. Res.* **2007**, *40*, 644–656.

(5) (a) Faul, C. F. J.; Antonietti, M. *Adv. Mater.* **2003**, *15*, 673–683. (b) Binnemans, K. *Chem. Rev.* **2005**, *105*, 4148–4204. (c) Ariga, K.; Hill, J. P.; Ji, Q. *Phys. Chem. Chem. Phys.* **2007**, *9*, 2319–2340. (d) Haketa, Y.; Sasaki., S.; Ohta, N.; Masunaga, H.; Ogawa, H.; Mizuno, N.; Araoka, F.; Takezoe, H.; Maeda, H. *Angew. Chem., Int. Ed.* **2010**, *49*, 10079–10083. (e) Wu, D.; Zhi, L.; Bodwell, G. J.; Cui, G.; Tsao, N.; Müllen, K. *Angew. Chem., Int. Ed.* **2007**, *46*, 5417–5420. (f) Wu, D.; Liu, R.; Pisula, W.; Feng, X.; Müllen, K. *Angew. Chem., Int. Ed.* **2011**, *50*, 2791–2794.

(6) (a) Kato, T. *Angew. Chem., Int. Ed.* **2010**, *49*, 7847–7848. (b) Ichikawa, T.; Yoshio, M.; Hamasaki, A.; Mukai, T.; Ohno, H.; Kato, T. *J. Am. Chem. Soc.* **2007**, *129*, 10662–10663. (c) Yoshio, M.; Mukai, T.; Ohno, H.; Kato, T. *J. Am. Chem. Soc.* **2004**, *126*, 994–995. (d) Shimura, H.; Yoshio, M.; Hoshino, K.; Mukai, T.; Ohno, H.; Kato, T. *J. Am. Chem. Soc.* **2008**, *130*, 1759–1765. (e) Yazaki, S.; Funahashi, M.; Kagimoto, J.; Ohno, H.; Kato, T. *J. Am. Chem. Soc.* **2010**, *132*, 7702–7708. (f) Tanabe, K.; Yasuda, T.; Yoshio, M.; Kato, T. *Org. Lett.* **2007**, *9*, 4271–4274. (g) Yazaki, S.; Funahashi, M.; Kagimoto, J.; Ohno, H.; Kato, T. *J. Am. Chem. Soc.* **2010**, *132*, 7702–7708.

(7) (a) Ma, K.; Lee, K.-M.; Minkova, L.; Weiss, R. G. *J. Org. Chem.* **2009**, *74*, 2088–2098. (b) Abdallah, D. J.; Robertson, A.; Hsu, H.-F.; Weiss, R. G. *J. Am. Chem. Soc.* **2000**, *122*, 3053–3062. (c) Chen, H.; Kwait, D. C.; Gönen, Z. S.; Weslowski, B. T.; Abdallah, D. J.; Weiss, R. G. *Chem. Mater.* **2002**, *14*, 4063–4072. (d) Ma, K.; Somashekhar, B. S.; Gowda, G. A. N.; Khetrapal, C. L.; Weiss, R. G. *Langmuir* **2008**, *24*, 2746–2758. (e) Ma, K.; Shahkhatuni, A. A.; Somashekhar, B. S.; Gowda, G. A. N.; Tong, Y. Y.; Khetrapal, C. L.; Weiss, R. G. *Langmuir* **2008**, *24*, 9843–9854. (f) Gowda, G. A. N.; Chen, H.; Khetrapal, C. L.; Weiss, R. G. *Chem. Mater.* **2004**, *16*, 2101–2106.

(8) (a) Hatano, T.; Kato, T. *Chem. Commun.* **2006**, 1277–1279. (b) Kimura, M.; Hatano, T.; Yasuda, T.; Morita, J.; Akama, Y.; Minoura, K.; Shimomura, K.; Kato, T. *Chem. Lett.* **2009**, *38*, 800–801.

(9) (a) Rashkin, M. J.; Hughes, R. M.; Calloway, N. T.; Waters, M. L. *J. Am. Chem. Soc.* **2004**, *126*, 13320–13325. (b) Rashkin, M. J.; Waters, M. L. *J. Am. Chem. Soc.* **2002**, *124*, 1860–1861.(c) Compared to **2a**′ (8.05 ppm), the significant downfield shift of H_d in **2a** (7.40 ppm) supports the shielding effect from the trisalkoxyphenyl ring at low concentrations. (d) In fact, the **3** series shows a downfield shift compared with the methyl derivative **3a**′ (H_a: 8.00 ppm; Supporting Information). The NOESY spectrum of **3a** did not show any coupling between H_h and H_a/H_d at low concentration (10^{-4} M, $CDCl_3$; see Supporting Information)

(10) (a) Dierking, I. *Texture of Liquid Crystals*; Wiley-VCH: Weinheim, 2003. (b) Demus, D.; Goodby, J.; Gray, G. W.; Spiess, H.-W.; Vill, V. *Handbook of Liquid Crystals*; Wiley-VCH: Weinheim, 1998.

(11) (a) Cardinaels, T.; Lava, K.; Goossens, K.; Elisseva, S. V.; Binnemans, K. *Langmuir* **2011**, *27*, 2036–2043. (b) Goossens, K.; Wellens, S.; Hecke, K. V.; Meervelt, L. V.; Cardinaels, T.; Binnemans, K. *Chem.—Eur. J.* **2011**, *17*, 4291–4306.

(12) (a) Kouwer, P. H. J.; Swager, T. M. *J. Am. Chem. Soc.* **2007**, *129*, 14042–1452. (b) Wiggins, K. M.; Kerr, R. L.; Chen, Z.; Bielawski, C. W. *J. Mater. Chem.* **2010**, *20*, 5709–5714.

(13) Hong, Y.; Lam, J. W. Y.; Tang, B. Z. *Chem. Commun* **2009**, 4332–4353.

(14) (a) Lakowicz, J. R. *Principles of Fluorescence Spectroscopy*, 3rd ed.; Springer: New York, 2006. (b) Valeur, B. *Molecular Fluorescence, Principles and Applications*, Wiley-VCH, Weinheim, 2002.

(15) Frisch, M. J.; et al. *Gaussian 03*, Revision E.01; Gaussian, Inc.: Wallingford, CT, 2007 (see Supporting Information for full reference).

(16) To assess the conformational effects on the $\sigma^*-\pi^*$ orbital coupling in the **1**, **2**, and **3** series, Mulliken charges at phosphorus have been calculated for both the optimized structures ("closed" and "open") and the crystal structures of the model compounds (different isomers). The calculations confirm the conformational effects on the Mulliken charge distribution at the phosphorus centers, and consequently the HOMO and LUMO energy levels. These results will be published elsewhere.

(17) (a) Sagara, Y.; Kato, T. *Nat. Mater.* **2009**, *4*, 605–610. (b) Sagara, Y.; Kato, T. *Angew. Chem., Int. Ed.* **2008**, *47*, 5175–5178. (i) Sagara, Y.; Yamane, S.; Mutai, T.; Araki, K.; Kato, T. *Adv. Funct. Mater.* **2009**, *19*, 1869–1875. (j) Zhang, G.; Lu, J.; Sabat, M.; Fraser, C. L. *J. Am. Chem. Soc.* **2010**, *132*, 2160–2162. (k) Nguyen, N. D.; Zhang, G.; Lu, J.; Sherman, A. E.; Fraser, C. L. *J. Mater. Chem.* **2011**, *21*, 8409–8415. (c) Yoon, S.-J.; Chung, J. W.; Gierschner, J.; Kim, K. S.; Choi, M.-G.; Kim, D.; Park, S. Y. *J. Am. Chem. Soc.* **2010**, *132*, 13675–13683. (d) Kunzelman, J.; Kinami, M.; Crenshaw, B. R.; Protasiewicz, J. D.; Weder, C. *Adv. Mater.* **2008**, *20*, 119–122. (e) Crenshaw, B. R.; Weder, C. *Chem. Mater.* **2003**, *15*, 4717–4724. (f) Löwe, C.; Weder, C. *Adv. Mater.* **2002**, *14*, 1625–1629. (g) Sagara, Y.; Mutai, T.; Yoshikawa, I.; Araki, K. *J. Am. Chem. Soc.* **2007**, *129*, 1520–1521. (h) Sase, M.; Yamaguchi, S.; Sagara, Y.; Yoshikawa, I.; Mutai, T.; Araki, K. *J. Mater. Chem.* **2011**, *21*, 8347–8354.